Journal of Molecular Catalysis B: Enzymatic 98 (2013) 138–144

Contents lists available at ScienceDirect

Journal of Molecular Catalysis B: Enzymatic

journal homepage: www.elsevier.com/locate/molcatb

Characterization of a highly thermostable ß-hydroxybutyryl CoA dehydrogenase from *Clostridium acetobutylicum* ATCC 824

Bettina Sommer, Daniel Garbe, Patrick Schrepfer, Thomas Brück*

Fachgebiet Industrielle Biokatalyse, Technische Universität München, Lichtenbergstr. 4, 85748 Garching, Germany

ARTICLE INFO

Article history:
Received 19 July 2013
Received in revised form 14 October 2013
Accepted 14 October 2013
Available online 22 October 2013

Keywords:
ß-Hydroxybutyryl CoA dehydrogenase
Clostridium acetobutylicum
Thermo stability
Solvent stability
Butanol production

ABSTRACT

Higher energy content and hydrophobicity make bio-based n-butanol a preferred building block for chemical and biofuels manufacturing. Butanol is obtained by *Clostridium* sp. based ABE fermentation process. While the ABE process is well understood, the enzyme systems involved have not been elucidated in detail. The important enzyme ß-hydroxybutyryl CoA dehydrogenase from *Clostridium acetobutylicum* ATCC 824 (Hbd) was purified and characterized. Surprisingly, Hbd shows extremely high temperature ($T > 60\,^{\circ}C$), pH (4–11) and solvent (1-butanol, isobutanol, ethanol) stability. Hbd catalyzes acetoacetyl CoA hydration to ß-hydroxybutyryl CoA up to pH 9.5, where the reaction is reversed. Substrate (acacCoA, ß-hbCoA) and cofactor (NADH, NAD^+, NADPH and $NADP^+$) specificities were determined. We identified NAD^+ as an uncompetitive inhibitor. Identification of process relevant enzymes such as Hbd is key to optimize butanol production via cellular or cell-free enzymatic systems.

1. Introduction

Butanol is a next generation renewable building block for the chemical and fuel sector due to its high energy content and hydrophobicity. Conventionally, bio-based butanol is produced via the *Clostridium acetobutylicum* based acetone (A), butanol (B) and ethanol (E) fermentation process [1,2]. However, the conventional ABE process suffers from marginal economic viability, low product titres due to end-product toxicities above 1–2% (v/v) [3] and the requirement to separate the different solvents via fractionated distillation.

To increase mass efficiency of the process recombinant 1-butanol-production has been realized in, i.e. *Escherichia coli* [4], *Bacillus subtilis* [5] and *Saccharomyces cerevisiae* [3] by cloning genetic elements for butanol biosynthesis into these microorganisms. However, to date this approach could hardly improve product yield. To obtain a mass and energy efficient butanol production process, it has been suggested to produce butanol using cell-free enzyme cascades [6]. This approach would potentially allow for much higher product yields and simplify downstream processing as we have recently shown for ethanol and isobutanol [7]. Key to a successful implementation of cell-free butanol production is the selection of process relevant enzyme complements with enhanced process stability and favourable catalytic properties.

However, while the physiology and genetics for ABE-biosynthesis is well understood, the concerted properties of the 14 enzyme systems involved in converting glucose to ABE have not been studies in detail.

An important enzyme in butanol biosynthesis is ß-hydroxybutyryl CoA dehydrogenase (Hbd; E.C. 1.1.1.157). Hbd catalyses the reversible reduction of acetoacetyl CoA (acacCoA) to ß-hydroxybutyryl CoA (ß-hbCoA) involving the cofactor NADH (Fig. 1) [4,8,9]. In our quest to select process relevant Hbd variants for butanol production, we applied genome mining tools to *C. acetobutylicum* ATCC 824 [10], which was one of the first strains used on an optimized ABE process.

At present, only uncertain catalytic data for *C. acetobutylicum* ATCC 824 Hbd (*Ca*-Hbd) (catalytic activity = 0.03 U/mg to 11.6 U/mg), derived from crude cell extracts, are available [4,8,11]. By contrast, some properties of the purified *Clostridium kluyveri* Hbd [12] and *Clostridium beijerinckii* (former "*C. butylicum*") NRRL B593 Hbd [13] have been described. While for *C. beijerinckii* Hbd pH dependence and kinetic constants for acacCoA, ß-hbCoA, NADH, NAD^+ and NADPH utilization are reported [13], data for *C. kluyveri* Hbd only state a dependence of NADPH as cofactor. Data for recombinant *Clostridium saccharobutylicum* (former *C. acetobutylicum*) Hbd only reported an activity with NADH as cofactor. On amino acid level *C. saccharobutylicum* and *C. beijerinckii* exhibit, 79% and 78% sequence identity compared with *C. acetobutylicum*, respectively, whereas *C. kluyveri* only possesses 69% identity.

More recently, the characterization of Hbd type FadB2 (ß-hydroxybutyryl-CoA dehydrogenase) from *Mycobacterium tuberculosis* was reported [9]. Conventionally, FadB (ß-hydroxyacyl-CoA

* Corresponding author. Tel.: +49 89 289 13253.
E-mail address: brueck@tum.de (T. Brück).

1381-1177/$ – see front matter © 2013 Elsevier B.V. All rights reserved.
http://dx.doi.org/10.1016/j.molcatb.2013.10.014

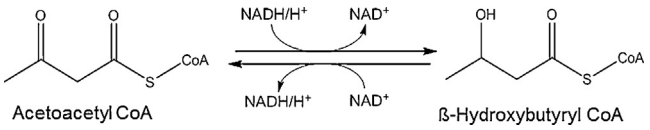

Fig. 1. Reaction catalyzed by Hbd from *C. acetobutylicum* ATCC 824.

dehydrogenase (E.C. 1.1.1.35)) catalyses the third step in ß-oxidation of fatty acid degradation and therefore preferentially catalyses the oxidation of ß-hbCoA to acacCoA. For the FadB2 isoenzyme cofactor specificities for NADH, NAD^+, NADPH and pH effects on catalysis have been described [9].

Although the amino acid sequence identity (43%) between FadB2 and *Ca*-Hbd is quite low, both enzymes are capable to perform the same reaction. However, in contrast to Hbd the reaction of FadB2 favours the conversion of ß-hbCoA to acacCoA, involved in fatty acid catabolism of the ß-oxidation pathway.

Structurally, the Hbd enzyme family has been poorly characterized.

To elucidate the full catalytic potential of elusive *Ca*-Hbd, this study focuses on comprehensive characterization of solvent, temperature and pH stability as well as substrate and cofactor specificities. The resulting data justify the utilization of the purified *Ca*-Hbd for construction of improved butanol production processes.

2. Materials and methods

2.1. Reagents, plasmid and strains

Restriction enzymes, klenow fragment, T4 ligase and T4 kinase were purchased from New England Biolabs (Frankfurt, Germany). Phusion polymerase was from Finnzymes (Espoo, Finland), deoxynucleotides from Rapidozym (Berlin, Germany). DNA and protein-standards were purchased from Thermo Scientific (Schwerte, Germany). DNA-sequencing was provided by GATC Biotech (Konstanz, Germany). Oligonucleotides were ordered from Thermo Scientific (Schwerte, Germany). AcacCoA and ß-hbCoA were purchased from Sigma–Aldrich (Taufkirchen, Germany).

Other chemicals as well as nicotinamide adenine dinucleotide disodium salt (NADH and NAD^+) were purchased from Carl Roth (Karlsruhe, Germany). 3-(Cyclohexylamino)-1-propanesulfonic acid (CAPS) and β-nicotinamide adenine dinucleotide phosphate tetrasodium salt (NADPH and $NADP^+$) were bought from AppliChem (Darmstadt, Germany).

E. coli BL21(DE3) (F^- *ompT hsdS*$_B$ ($r_B^-m_B^-$) *gal dcm* (DE3)) was purchased from Merck (Darmstadt, Germany).

2.2. Structural modelling of Ca-Hbd and molecular dynamics simulations

2.2.1. Structural modelling of Ca-Hbd

We have used HHpred server [14] and the Yasara bioinformatics suite to model the *Ca*-Hbd structure. Modelling was conducted according to manufacturer's protocols and official guidelines.

2.2.2. Temperature and pH dependent molecular dynamics simulations

Molecular dynamics (MD) simulations employed the Yasara software suite using the AMBER99 force field [15]. The system was composed of the HHpred modelled *Ca*-Hbd structure, immersed in a rectangular TIP3P water box with a 10 Å buffer. Sodium chloride adjusted to a 0.1 molar concentration balanced the electrostatic charge associated with the protein. Periodic boundary conditions were applied, while the Particle-mesh Ewald algorithm was used for the calculation of long range electrostatic interactions. The time step for intramolecular forces was chosen to be 1.25 fs. The cut-off for non-bonded van der Waals interactions was 10 Å. For temperature and pH dependent simulations, 1300 steepest decent minimizing were coupled to simulated annealing steps preceding the productive 1 ns MD run. Data resulting from the MD simulations were primarily analyzed by Yasara. Using these MD boundaries, temperature dependent protein unfolding simulations were carried out at 85 °C using the modelled *Ca*-Hbd structure with omitted substrate. In analogy structural changes occurring at pH 5, 7 and 10 were determined using the modelled *Ca*-Hbd structure in the presence of the substrate acacCoA.

2.3. Cloning

The *Ca-hbd* gene (GeneBank No. AE001437.1) was cloned into the *E. coli*-compatible vector pCBRHisC [7] using *Bfua*I and *Bsa*I restriction sites. For amplification of *Ca-hbd* the upstream primer 5′-CAGCAAGGTCTCTCATATGAAAAAGGTATGTGTTATAGGT (*Bfua*I restriction site underlined) and the downstream primer 5′-TTTTGAATAATCGTAGAAACCTTTTCCT GATTTTCTTCC were used.

2.4. Heterologous expression and enzyme purification for enzymatic assays

Enzyme expression was performed using *E. coli* BL21 (DE3) as host strain. *Ca*-Hbd was expressed in LB media supplemented with 50 μg/ml kanamycin. After inoculation cells were grown to OD_{600} = 0.5–0.7 at 37 °C and subsequently induced with 1 mM isopropyl-ß-D-thiogalactopyranoside (IPTG). For further cultivation, the temperature was lowered to 25 °C for 20 h. Cell lysates were prepared with Emulsiflex-B15 (Avestin, Mannheim, Germany), cell debris was removed by centrifugation (21,000 × g, 4 °C, 20 min) (Fig. S1). Protein purification was performed using Ni^{2+}-NTA resin. Desalting of the proteins was performed with PD-10 columns (GE Healthcare, Munich, Germany). Protein concentration was measured at 280 nm with unfolded protein in 8 M Urea [16]. The necessary extinction coefficient was calculated by the ExPASY ProtParam tool [17].

2.5. Enzyme assays

Activity of *Ca*-Hbd was measured at 340 nm via monitoring the depletion or formation of NADH and NADPH, respectively. The assays were performed in a microtiter plate format using a monochromator equipped plate reader (Enspire, Perkin Elmer, Rodgau, Germany). The reaction mixture excluding the protein was incubated at the measured temperature. Hence, the pH-values of all buffers were adjusted to the desired temperature according to Stoll and Blanchard [18]. All controls and each enzymatic reaction were performed in triplicate. In doing so, one unit of enzyme activity was defined as the amount of enzyme necessary to convert 1 μmol substrate per minute.

For the thermal-stability-assays, *Ca*-Hbd was stored over several days at 40 °C, 50 °C, 60 °C, 70 °C and 80 °C in a water bath. Subsequently the assays were performed in reaction mixtures containing 50 mM Hepes (pH 7 at current temperature), 0.3 mM acacCoA and 0.3 mM NADH. Reaction mixtures for the determination of temperature optima were prepared accordingly. Up to 65 °C activities were determined at its current temperature. Measurements above 65 °C were done by incubating *Ca*-Hbd in a heating block for 15 min followed by activity determinations at 50 °C.

For solvent-stability-assays, reaction mixtures contained 50 mM Hepes (pH 7 at 50 °C), 0.3 mM acacCoA, 0.3 mM NADH and 1-butanol (0–10%), ethanol (0–20%) or isobutanol (0–10%). All assays were performed at 50 °C.

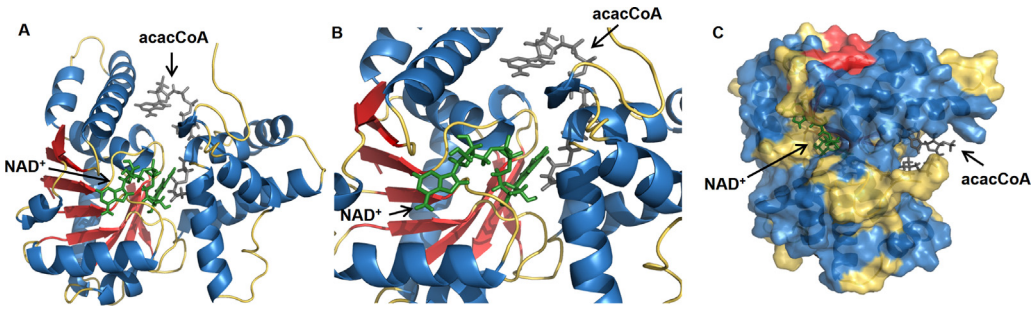

Fig. 2. Modelled *Ca*-Hbd structure. (A) Structural overview with the substrate acacCoA and NAD^+ as cofactor, (B) active site and (C) surface of *Ca*-Hbd. The Rossmann fold is marked as ß-sheets.

During the determination of pH-optima, a sodium acetate buffer was applied for the pH-range 4–6, Tris buffer for pH 7–9 and Caps buffer for pH 10–11 at 50 °C. The reaction mixtures contained 50 mM of current buffer, 0.3 mM acacCoA and 0.3 mM NADH or 0.6 mM ß-hbCoA and 0.3 mM NAD^+/$NADP^+$.

2.6. Kinetics of Ca-Hbd

Ca-Hbd was added with a final concentration of 0.75 μg/ml to the reaction mixture, which contained 50 mM Hepes (pH 7 at 50 °C) and 50 mM Caps (pH 10 at 50 °C), respectively. In case of the K_M determination for NADPH the *Ca*-Hbd concentration was increased to 9.4 μg/ml.

CoA substrates and cofactor amounts applied were 0.4 mM acacCoA, 0.8 mM ß-hbCoA, 0.3 mM NADH and 0.3 mM NAD^+, respectively. For the inhibition studies, different amounts of NAD^+ were added to the reaction mixture. The kinetic parameters K_M, v_{max} and k_{cat} for each substrate and cofactor were determined by varying their concentrations and fitting the data to the Michaelis–Menten equation by using Sigma Plot 12.5.

2.7. Circular dichroism (CD) measurements

CD spectra were obtained with a JASCO spectropolarimeter, model J-715 (JASCO International Co., Tokyo, Japan). A quartz cuvette exhibiting a light path lengths of 0.1 cm and for temperature regulation a thermocouple (JASCO) was used. *Ca*-Hbd was dissolved in 50 mM NaPi buffer (pH 7 at 20 °C) at a concentration of 0.21 mg/ml. All obtained spectra were corrected for buffer contributions and the final spectrum represents the average of 16 scans.

Also the *Ca*-Hbd temperature dependence was analyzed at 225 nm. During these experiments the temperature was increased by a ramp of 0.75 °C/min using a Peltier thermocouple.

3. Results and discussion

3.1. Structural characterization of Ca-Hbd

At present, no crystal structure of a microbial Hbd involved in butanol biosynthesis is available. Based on primary sequence *Ca*-Hbd shows 44% identity to a probable Hbd from *E. coli* K12 (pdb ID: 3MOG), for which a crystal structure is reported. However, the *E. coli* protein is involved in fatty acid catabolism and not in butanol formation. Additionally, the two proteins show only minor convergence in secondary structure features. To identify a suitable structural scaffold for *Ca*-Hbd we applied multiple sequence profile alignments with the *Ca*-Hbd template using the HHpred server, which employs profile Hidden Markov Models [14]. The selected protein scaffolds for sequence alignment and structure modelling gave e-values of 9×10^{-55}–3.6×10^{-55}, with *Homo sapiens* Hbd showing the highest secondary structural similarity. Interestingly, the *Homo sapiens* Hbd catalyses the same reaction as *Ca*-Hbd [19]. Using the alignment data and structure prediction tools of the HHpred server, we were able to create a high quality *Ca*-Hbd model. Subsequently, we applied the MUSTANG algorithm [15] of the Yasara bioinformatics suite to carry out an almost complete tertiary structural alignment of *Ca*-Hbd with the *Homo sapiens* Hbd scaffold (pdb ID: 1F0Y). The tertiary structure alignment between the two enzymes resulted in an RMSD (root mean square deviation) value of 0.324 Å over 277 aligned amino acid residues with an overall 45.49% primary sequence identity. In the resulting high quality *Ca*-Hbd model substrate and cofactor positions were adopted from structural data of human 3-hydroxyacyl CoA dehydrogenase (Fig. 2). The structure of *Ca*-Hbd represents a typical α/ß fold enzyme, which is dominated by α-helical bundles that are linked by several unordered loops (Fig. 2A). Much like other NADH/NADPH dependent dehydrogenases *Ca*-Hbd features an extended ß-sheet domain, which contains the Rossmann fold topology crucial for cofactor binding (Fig. 2A and B) [20]. *Ca*-Hbd features opposing binding sites for each the acacCoA substrate and NADH cofactor, respectively. The cofactor NADH is oriented perpendicular to the acacCoA substrate, which potentially aids electron transfer during acacCoA reduction (Fig. 2B). *Ca*-Hbd is a globular protein with minimized solvent accessibility (Fig. 2C). Both NADH and acacCoA are situated in binding pockets, which are only partially shielded against the solvent, which may influence their stability under extreme pH and temperature conditions. To further elucidate these effects we have applied biochemical methods and state of the art molecular dynamics simulations to compliment experimental observations.

3.2. Biochemical characterization of Ca-Hbd

3.2.1. Determination of pH optima

To compare the pH effects of *Ca*- and *C. beijerinckii* Hbd for the native acacCoA reduction and the reversible ß-hbCoA oxidation we examined both reactions over a broad range of pH-values, using an established NADH assay [8,13].

The pH effects of the *Ca*-Hbd reaction with acacCoA and ß-hbCoA as substrates were studied at 50 °C (Fig. 3).

The conventional reduction of acacCoA to ß-hbCoA occurs over a wide pH range between 4 and 10 with a pH_{opt} at 5. By contrast, the reverse reaction, oxidation of ß-hbCoA to acacCoA with NAD^+ as cofactor is catalyzed only within a small pH-range of 9.5–10.5 (Fig. 3) with a maximum at 10. The pH dependence of Hbd reaction can be correlated with the physiology of microbial solventogenesis. In the primary fermentation phase (acidogenesis) clostridia produce acids (i.e. acetate, butyrate) thereby lowering media's pH. Subsequently, the external pH of the medium shifts below 5 triggering clostridial metabolism to switch on solvent production [21–25]. Therefore, synergies between the pH profile of Hbd and

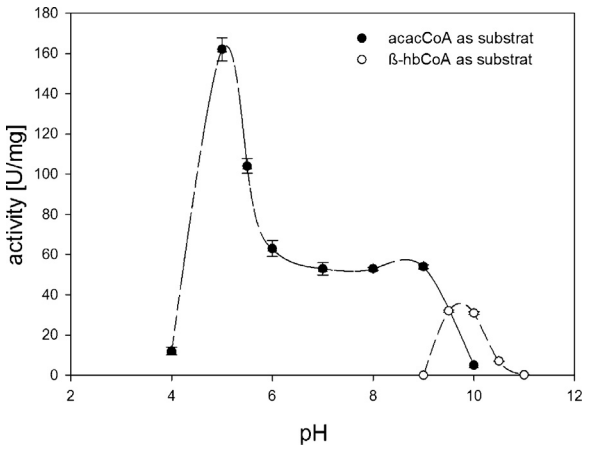

Fig. 3. Effect of pH on the Hbd catalyzed reactions. 50 mM sodium acetate buffer was used for pH 4–6, 50 mM Tris buffer for pH 7–9 and 50 mM Caps buffer for pH 10–11 at 50 °C. Each activity is the mean of three repilciates.

the microbial physiology are essential for solvent production. This notion is further corroborated by the fact that pH profiles of acac-CoA and ß-hbCoA conversion are almost identical between the Hbd enzymes from *C. acetobutylicum* and *C. beijerinckii*, respectively.

To further clarify the pH effects on the reactivity of *Ca*-Hbd we have used MD simulations to elucidate potential energy minimized structural changes of the enzyme at pH 5 and 10, respectively. The structural overlay of pH dependent *Ca*-Hbd conformations (Fig. S2A) indicates only minor overall distortions in the enzyme structure. The calculated structural changes at pH 5 compared to pH 10 can be quantified by an RMSD value of 1.68 Å. However, two outer α-helical domains, linked by a short loop (Fig. S2B), are responsible for substrate binding and are slightly twisted at pH 10. This structural change results in a significant reorientation of the CoA moiety of the substrate. This substrate repositioning in the active site may contribute to the preference for ß-hbCoA oxidation observed at pH 10. Hence, the MD simulations support biochemical data on pH dependent reaction reversal.

3.2.2. Determination of temperature optima and half-life

For a stable butanol production process the application of highly stable enzyme systems to achieve relevant production rates are required [7]. Therefore, we closely examined the thermostability of *Ca*-Hbd.

A temperature dependent profile for the reaction of *Ca*-Hbd with acacCoA and NADH as co-substrate is shown in Fig. 4A. The temperature rise from 25 °C to 60 °C resulted in a 1.5-fold increase of activity (Fig. 4A). At T_{opt} (65 °C) an activity of 109 (±15) U/mg was observed. Above 65 °C *Ca*-Hbd activity gradually decreased.

The concurrent CD measurements supported the activity profile, since protein unfolding was not observed up to 65 °C (Fig. 4A and B). Above 65 °C structural unfolding was detected with a terminal unfolding point at 85 °C. Based on this data a T_m of 79 °C was calculated.

Relevant activities for *Ca*-Hbd over extended timeframes ($t \leq 380$ h) could be determined at 40 °C, 50 °C, 60 °C, 70 °C and 80 °C, respectively (Table 1), indicating that *Ca*-Hbd is a highly thermostable enzyme. Interestingly, no definitive half-life could be determined for *Ca*-Hbd in the temperature range of 40–60 °C even after 380 h (~16 days). In this timeframe enzyme activity still remained in the range of 62% (40 °C and 50 °C) to 67% (60 °C) with respect to the starting values.

By contrast, at 70 °C the *Ca*-Hbd half-life activity could be observed after 42 h. Further, at 80 °C the half-life was reached in less than 1 h, indicating irreversible protein unfolding which was

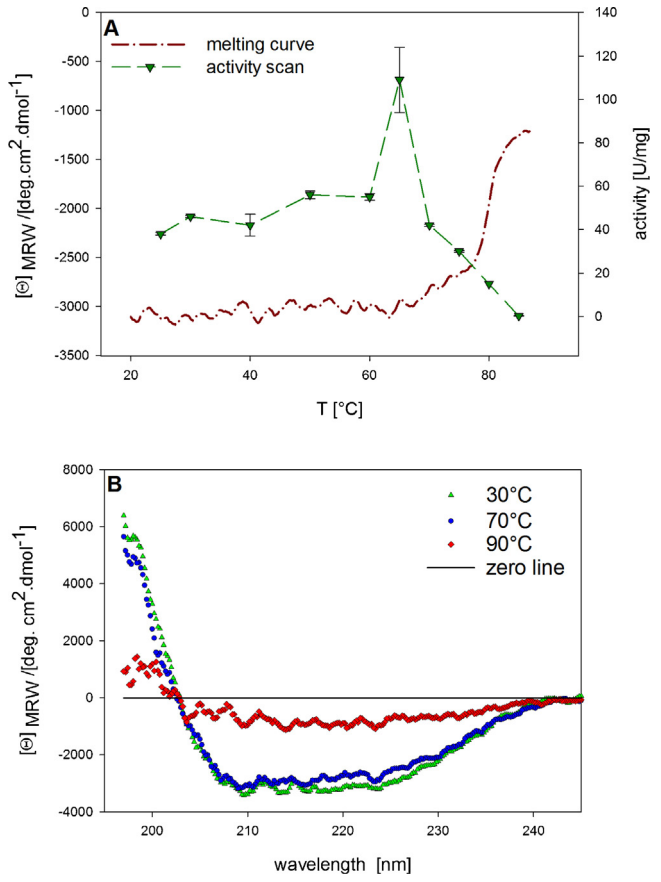

Fig. 4. Determination of temperature optimum and thermostability of *Ca*-Hbd. Enzyme assays were performed in a range from 25 °C to 85 °C. (A) Temperature wavelength scan from 10 °C to 90 °C (heating rate: 0.75 °C/min) at 225 nm was obtained via CD spectrometer. (B) Superimposed CD-spectra of the temperature wavelength scan of *Ca*-Hbd at 30 °C, 70 °C and 90 °C. Every 20 °C a complete wavelength scan was carried out. Values of CD spectroscopy are presented in mean residue ellipticity ($[\Theta]_{MRW}$).

confirmed by CD measurements (Fig. 4A). To our knowledge this is the first account of *Ca*-Hbd being an extremely thermostable enzyme.

To further elucidate the structural features providing the pronounced *Ca*-Hbd thermostability we applied MD simulations to virtually expose *Ca*-Hbd to 80 °C over a defined time period. Comparing the time dependent structural models indicate a significant decrease of solvent exposed outer α-helical domains ($t_0 = 51.8\% \rightarrow t_{final} = 34.8\%$) and their conversion to unfolded turns ($t_0 = 8.2\% \rightarrow t_{final} = 19.1\%$) and coil topologies ($t_0 = 21.6\% \rightarrow t_{final} = 29.1\%$). These structural changes resulted in an increase of the calculated accessible surface area ($t_0 = 13120.42$ Å $\rightarrow t_{final} = 13172.4$ Å), consistent with partial unfolding of solvent exposed protein structures. In contrast, buried protein structures, such as the extended ß-sheet domain, harbouring the catalytically relevant Rossmann fold and were protected

Table 1
Half-life activity of *Ca*-Hbd at 40 °C, 50 °C, 60 °C, 70 °C and 80 °C, respectively. The remaining activity in per cent after 380 h is specified in the 3rd column.

T [°C]	Half-life [h]	A_{0h}/A_{380h} [%]
40	/	62
50	/	62
60	/	67
70	42	/
80	0.9	/

Table 2
Kinetic parameters of *Ca*-Hbd. The standard deviation is stated in parentheses.

	V_{max} [U/mg]	K_M [mM]	K_{cat} [s^{-1}]	K_{cat}/K_M [$M^{-1}\ s^{-1}$]
Acetoacetyl CoA	75.7 (±2.7)	0.11 (±0.01)	38.6 (±1.3)	3.5 (±0.2) × 10^5
ß-Hydroxybutyryl CoA	53.3 (±1.2)	0.29 (±0.01)	27.1 (±0.6)	9.4 (±0.1) × 10^4
NADH	61.5 (±2.9)	0.14 (±0.02)	31.4 (±1.4)	2.3 (±0.2) × 10^5
NAD^+	55.1 (±1.9)	0.27 (±0.02)	28.1 (±0.9)	1.0 (±0.4) × 10^5
NADPH	3.31 (±0.27)	0.45 (±0.07)	1.7 (±0.1)	3.8 (±0.4) × 10^3

from unfolding (t_0 = 16.7% → t_{final} = 15.2%). The preservation of buried structures of the enzyme active site provides extended catalytic activity of *Ca*-Hbd at elevated temperatures. Therefore, MD simulations corroborate biochemical and biophysical data on thermostability of *Ca*-Hbd.

From a process-engineering perspective the extended thermostability of *Ca*-Hbd would provide extended operation capacity and reduced enzyme costs in an optimally balanced, cell-free butanol production process.

3.2.3. Determination of catalytic properties

To elucidate the catalytic properties of *Ca*-Hbd the kinetic constants, substrate and cofactor specificities were determined. Here we particularly focused on defining the catalytic limits of the pH dependent, reversible acacCoA reduction. For the first time this study reports a comprehensive substrate and cofactor dependence of a *Ca*-Hbd involved in butanol biosynthesis.

3.2.3.1. Substrate specificities. When measured at its respective pH optimum, the *Ca*-Hbd catalyzed acacCoA reduction (162 (±6) U/mg) is 5 times faster than the ß-hbCoA oxidation (31 U/mg; Fig. 3). Interestingly, assay data obtained at equal concentrations of ß-hbCoA and NAD^+, indicated that only 50% of the substrate was converted during the reaction. Since commercial ß-hbCoA is a racemic mixture, this data suggests that only a single enantiomer is an active reactant. It has previously been reported that *E. coli* Hbd is selective for the (S)-stereoisomer [11]. It is therefore reasonable that also *Ca*-Hbd is specific for the (S)-enantiomer of ß-hbCoA.

The kinetic data shown in Table 2 summarizes *Ca*-Hbd properties for specific reactions with acacCoA, ß-hbCoA, NADH, NAD^+ and NADPH, respectively.

In line with the previous observation K_M value of the *Ca*-Hbd reaction with its native substrate acacCoA (K_M = 0.11 (±0.01) mM) was one third of the value observed with ß-hbCoA (K_M = 0.29 (±0.01) mM), which indicates a higher binding capacity of acacCoA to the enzymes active site. Additionally, we have examined *Ca*-Hbd cofactor specificities. Again *Ca*-Hbd shows a greater binding capacity to the reductant NADH (K_M = 0.14 (±0.02) mM) compared to the oxidant NAD^+ (K_M = 0.27 (±0.02) mM), which indicates that the native enzyme significantly favours the reduction of acacCoA. Therefore, the reaction of acacCoA towards ß-hbCoA is both kinetically and thermodynamically (ΔG^0 = −3.76 kcal/mol [26]) favoured, which drives the overall reaction towards butanol production instead of fatty acid catabolism as observed for FadB2 [9]. We have collected our kinetic data series at pH 7, which is just above the pH optimum (pH_{opt} 5) of *Ca*-Hbd. The main reasoning for this experimental set-up was the enhanced stability of NADH at neutral pH and the downstream opportunity to create a butanol targeted enzyme cascade, which takes pH requirements of other enzyme systems into account.

By contrast, reports on the catalytic properties of *C. beijerinckii* Hbd have measured kinetics at the pH optimum for acacCoA reduction (pH 5.5) and ß-hbCoA oxidation (pH 9), respectively. Additionally, reactions for *C. beijerinckii* Hbd were recorded at 26 °C, compared to 50 °C applied in this study. Therefore, a direct comparison of kinetic data for *Ca*-Hbd and *C. beijerinckii* Hbd is limited. Nevertheless, the specifity constant for acacCoA reduction was about 1000-fold higher in *C. beijerinckii* Hbd (k_{cat}/K_M = 1.3 × 10^8 M^{-1} s^{-1}) compared to *Ca-Hbd* (k_{cat}/K_M = 3.5 × 10^5 M^{-1} s^{-1}), while the respective K_M value was 10-fold lower in *C. beijerinckii* Hbd (K_M = 0.014 mM) compared to *Ca*-Hbd (K_M = 0.11 mM), respectively. This data set indicates that *C. beijerinckii* Hbd has an improved catalytic efficiency and substrate binding compared to *Ca*-Hbd under the respective experimental conditions.

3.2.3.2. Cofactor specificities. To obtain a comprehensive data set on the cofactor dependence for *Ca*-Hbd we have examined the reaction with NADH, NAD^+, NADPH and $NADP^+$ (Table 2 and Fig. S3).

Initial experiments indicate that *Ca*-Hbd has a clear preference towards NADH as cofactor, since corresponding reactions with NADPH resulted in an 18-fold decrease in activity. This trend was mirrored in the catalytic efficiency constants (k_{cat}/K_M) for the NADH- (k_{cat}/K_M = 2.3 (±0.2) × 10^5 M^{-1} s^{-1}) and NADPH-linked reaction (k_{cat}/K_M = 3.8 (±0.4) × 10^3 M^{-1} s^{-1}), respectively. This suggests that NADH is the physiological co-substrate of *Ca*-Hbd. When the reverse (oxidative) reaction with ß-hbCoA was examined, NAD^+ (k_{cat}/K_M = 1.0 (±0.4) × 10^5 M^{-1} s^{-1}) was preferred over $NADP^+$, whose activity was so low (catalytic activity = 0.005 (±0.001) U/mg) that no catalytic constants could be determined. A direct activity comparison indicates that NAD^+ (catalytic activity = 55.1 (±1.9) U/mg) reacts 11,000 times faster than $NADP^+$.

The same cofactor preference was observed for FadB2 from *M. tuberculosis* [9]. While the cofactor preference of *Ca*-Hbd mirrors that of *C. beijerinckii* Hbd, literature reports for *C. saccharobutylicum* Hbd a very selective preference only for NADH as cofactor [27]. On the contrary, *C. kluyveri* Hbd only accepts NADPH as its cofactor [12].

3.2.3.3. Ca-Hbd cofactor and substrate inhibition. Kim and Copeland reported the characterization of *Rhizobium* sp. strain CC 1192 acetyl CoA acetyltransferase using a coupled enzyme reaction with commercial 3-hydroxyacyl CoA dehydrogenase [28]. Their study eludes that accumulation of NAD^+ concentrations greater than 0.5 mM in the reaction may lead to Hbd inhibition.

In this study we quantified this inhibitory effect for the first time. The effect of product (NAD^+) inhibition on the NADH dependent acacCoA reduction to ß-hbCoA was considered using steady-state kinetic data (Fig. 5).

For each of the examined NAD^+ concentrations (0–10 mM NAD^+) the K_M and v_{max} values of the respective reactions decrease continuously. In the absence of NAD^+, K_M and v_{max} values in the order of 0.11 (±0.01) mM and 75.7 (±2.70) U/mg were observed (Table 2). By contrast, addition of 10 mM NAD^+ respective K_M and v_{max} values were reduced to 0.03 (±0.005) mM and 13.04 (±0.39) U/mg, respectively.

The double-reciprocal plot of v_0 plotted versus the concentration of acacCoA results in a set of parallel lines (Fig. 5), which allows deduction of a K_i value of 2.0 mM for NAD^+ addition. Kinetic data indicates that NAD^+ acts as an uncompetitive inhibitor, suggesting that *Ca*-Hbd contains two distinct binding sites, for acacCoA/ß-hbCoA and the cofactor pair NADH/NAD^+, respectively. Therefore,

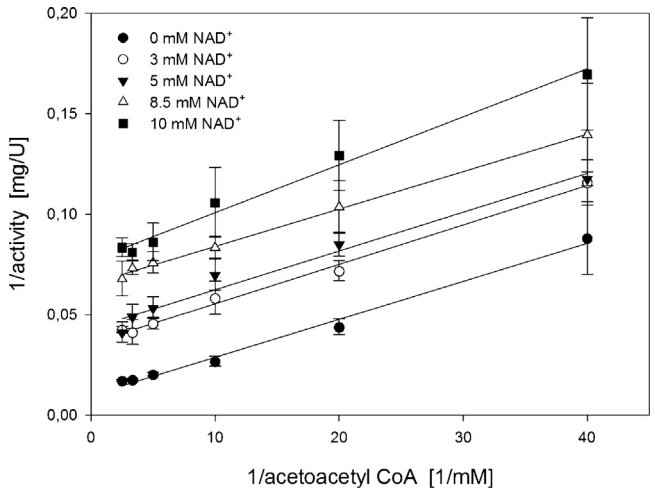

Fig. 5. Steady state kinetic characterization of *Ca*-Hbd. Double-reciprocal plots monitoring NAD^+ product inhibition with respect to NADH. Each activity is the mean of three repilcates.

the kinetic data set for NAD^+ inhibition is consistent with current structural model of *Ca*-Hbd (Fig. 2).

Colby and Chen reported that *C. beijerinckii* Hbd is inhibited by acacCoA at concentrations as low as 20 μM [13]. Their study showed that the substrate inhibition can be relieved by addition of NADH concentrations in excess of 20 μM. In this study a similar effect could be observed. However, for *Ca*-Hbd a slight decrease in activity could also be determined when NADH was supplied at limiting concentrations (data not shown).

3.2.3.4. Determination of solvent tolerance. In order to construct efficient butanol production systems, enzymes with high solvent tolerance are required. This study examined the solvent tolerance of the Hbd enzyme family for the first time. Consequently, *Ca*-Hbd was also tested for its stability towards the process relevant alcohols ethanol, butanol and isobutanol [7]. Hbd retained 50% activity in the presence of 20% (v/v) ethanol, 9% (v/v) butanol and 10% (v/v) isobutanol (Fig. S4). The significant solvent tolerance of *Ca*-Hbd is of particular process relevance for both cell and cell-free butanol production methods.

C. acetobutylicum ATCC 824 can produce 7.9 g/l butanol, whereas *C. acetobutylicum* NRRL B591 only produces 2.6 g/l butanol [29]. Thus *C. acetobutylicum* ATCC 824 belongs to the best butanol production strains, but its growth is inhibited by 50% at 0.9% (v/v) butanol. By a stepwise enrichment procedure a more butanol-tolerant mutant was found, which growth is halved by 1.9% (v/v) butanol [29]. Hbd from *C. acetobutylicum* ATCC 824 remains 44% of its native activity at even 10% (v/v) butanol and 50 °C. Furthermore, at butanol concentrations above 10% (v/v) (20 °C) a biphasic butanol/water system is formed spontaneously. Within the biphasic system *Ca*-Hbd's activity could easily increase again, because most butanol is removed from the water phase and subsequently accumulated in the upper organic phase. Therefore, decreased influence of the product's toxicity as observed for *Ca*-Hbd, is an outstanding process advantage particularly when cell-free enzyme cascades are applied for butanol production [30].

4. Conclusions

Butanol is a next generation building block for renewable chemical and biofuel processes due to its enhanced energy content and hydrophobicity compared to first generation fuels such as ethanol. Current, cell-based butanol production systems are not mass efficient due to side products (ethanol and acetone). Additionally, these cell based systems are limited in their productivity due to end-product toxicities. An alternative to cell-based production approaches are cell-free enzyme cascades which potentially can convert monomeric sugars into butanol with much higher yields. Subsequently, these features allow for simplified, energy efficient product recovery [7]. However, both robust cell and cell-free production systems require upstream identification of process relevant enzyme systems, which preferentially show enhanced solvent and thermostability as well as good catalytic features. Although the physiology of cell based butanol production has been investigated in detail, the enzyme systems involved in butanol production have only been marginally characterized both structurally and biochemically. This study focused on identification and correlation of biochemical and structural features of the *Ca*-Hbd, an important enzyme in butanol biosynthesis. We have applied state of the art structural modelling procedures to create a high quality model of *Ca*-Hbd. To our knowledge this is the first structural model of the microbial Hbd family, involved in butanol biosynthesis. The enzyme structure shows a globular overall structure with maximal packing of secondary structure. As with all NADH dependent dehydrogenases, Hbd harbours a Rossmann binding domain, which is embedded into an extended ß-barrel fold. The substrate binding site located in a linked α-helical domain, which is placed opposite the cofactor binding site. Subsequently, we have attempted to correlate Hbd biochemical properties to its structural features. This is the account of catalytic features of a purified, recombinant *Ca*-Hbd capable of the reversible, pH dependent reduction of acacCoA over a pH range of 5–9. The reverse reaction with ß-hbCoA occurs only at pH 9–11 and is 5 times slower than the reaction with acacCoA. This suggests that *Ca*-Hbd preferentially acts in butanol synthesis direction and is not part of the ß-oxidation catabolism of the fatty acid, where ß-hbCoA is a key intermediate. The catalytic constants indicate that the enzyme shows a clear preference to NADH/NAD^+ as a cofactor, while only residual activity with NADPH could be observed. Interestingly, we could identify NAD^+ as a non-competitive inhibitor of the Hbd reaction with acacCoA. This indicates that in butanol biosynthesis acacCoA conversion to ß-hbCoA is tightly controlled. Therefore, in any cell-free butanol biosynthesis approach the substrate flux from the master intermediate acetylCoA over acacCoA to ß-hbCoA requires definitive cofactor balancing to enable efficient conversion of respective CoA intermediates towards butanol as the end product. The kinetic data for NAD^+ inhibition indicates that the enzyme has distinct binding sites, for cofactor and substrate, respectively. This data was consistent with the structural features of our Hbd model. Next to comprehensive characterization of *Ca*-Hbd substrate and cofactor specificities, we have characterized the thermo- and solvent stability of the enzyme family for the first time. Interestingly, *Ca*-Hbd is extremely thermostable with an apparent T_m of 79 °C and an activity half of 1 h at 80 °C. Further, *Ca*-Hbd is surprisingly solvent stable. At butanol concentrations up to 10% (v/v) 45% activity are remaining over extended time periods. Together features such as thermo- and solvent stability are extremely important for enzyme systems to be selected for targeted cell and cell-free butanol production systems. Therefore, *Ca*-Hbd is an excellent candidate for creating improved biotechnological butanol production processes. Additionally, at 10% (v/v) butanol forms a biphasic system with water, which would allow simple gravimetric separation of the butanol product from the aqueous reaction phase. The pronounced thermo- and solvent stability of *Ca*-Hbd is routed in its compact, globular protein structure, which we could demonstrate using our Hbd model.

Acknowledgements

Plasmids were kindly provided by Prof. V. Sieber (Chair of Chemistry of Biogenic Resources, Technische Universität München, Germany) and Clariant. Especially, we thank Prof. J. Buchner and Eva Herold (Chair in Biotechnology, Technische Universität München, Germany) for accessing the JASCO spectropolarimeter J-715 and helpful support during the experiments.

This work was supported by the German Federal Ministry of Education and Research (BMBF) through grant No. 0315485B and Clariant, a for-profit company pursuing commercialization of bio-based processes.

B.S. and D.G. drafted the manuscript. TB conceived this study and finalized the manuscript. B.S. conducted the cloning, enzyme production and characterization. P.S. modelled the Ca-Hbd structure.

Appendix A. Supplementary data

Supplementary data associated with this article can be found, in the online version, at http://dx.doi.org/10.1016/j.molcatb.2013.10.014.

References

[1] P. Dürre, Appl. Microbiol. Biotechnol. 49 (1998) 639–648.
[2] D.T. Jones, D.R. Woods, Microbiol. Rev. 50 (1986) 484–524.
[3] E.J. Steen, R. Chan, N. Prasad, S. Myers, C.J. Petzold, A. Redding, M. Ouellet, J.D. Keasling, Microb. Cell Fact. 7 (2008) 36.
[4] M. Inui, M. Suda, S. Kimura, K. Yasuda, H. Suzuki, H. Toda, S. Yamamoto, S. Okino, N. Suzuki, H. Yukawa, Appl. Microbiol. Biotechnol. 77 (2008) 1305–1316.
[5] D.R. Nielsen, E. Leonard, S.H. Yoon, H.C. Tseng, C. Yuan, K.L. Prather, Metab. Eng. 11 (2009) 262–273.
[6] Y.H. Zhang, Biotechnol. Bioeng. 105 (2010) 663–677.
[7] J.K. Guterl, D. Garbe, J. Carsten, F. Steffler, B. Sommer, S. Reisse, A. Philipp, M. Haack, B. Rühmann, A. Koltermann, U. Kettling, T. Brück, V. Sieber, ChemSusChem 5 (2012) 2165–2172.
[8] Z.L. Boynton, G.N. Bennet, F.B. Rudolph, J. Bacteriol. 178 (1996) 3015–3024.
[9] R.C. Taylor, A.K. Brown, A. Singh, A. Bhatt, G.S. Besra, Microbiology 156 (2010) 1975–1982.
[10] J. Nölling, G. Breton, M.V. Omelchenko, K.S. Makarova, Q. Zeng, R. Gibson, H.M. Lee, J. Dubois, D. Qiu, J. Hitti, Y.I. Wolf, R.L. Tatusov, F. Sabathe, L. Doucette-Stamm, P. Soucaille, M.J. Daly, G.N. Bennett, E.V. Koonin, D.R. Smith, J. Bacteriol. 183 (2001) 4823–4838.
[11] S.H. Lee, S.J. Park, S.Y. Lee, S.H. Hong, Appl. Microbiol. Biotechnol. 79 (2008) 633–641.
[12] V.K. Madan, P. Hillmer, G. Gottschalk, Eur. J. Biochem./FEBS 32 (1973) 51–56.
[13] G.D. Colby, J.S. Chen, Appl. Environ. Microbiol. 58 (1992) 3297–3302.
[14] J. Söding, A. Biegert, A.N. Lupas, Nucleic Acids Res. 33 (2005) W244–W248.
[15] A.S. Konagurthu, J.C. Whisstock, P.J. Stuckey, A.M. Lesk, Proteins 64 (2006) 559–574.
[16] M.R. Connor, J.C. Liao, Curr. Opin. Biotechnol. 20 (2009) 307–315.
[17] E. Gasteiger, C. Hoogland, A. Gattiker, S.e. Duvaud, M. Wilkins, R. Appel, A. Bairoch, in: J. Walker (Ed.), The Proteomics Protocols Handbook, Humana Press, Totowa, 2005, pp. 571–607.
[18] V.S. Stoll, J.S. Blanchard, Guide to Protein Purification, vol. 466, Elsevier Academic Press Inc, Sang Diego, 2009, pp. 43–56.
[19] J.J. Barycki, L.K. O'Brien, A.W. Strauss, L.J. Banaszak, J. Biol. Chem. 275 (2000) 27186–27196.
[20] M. Nardini, B.W. Dijkstra, Curr. Opin. Struct. Biol. 9 (1999) 732–737.
[21] G.J. Thorn, J.R. King, S. Jabbari, Math. Biosci. 241 (2013) 149–166.
[22] E.T. Papoutsakis, Curr. Opin. Biotechnol. 19 (2008) 420–429.
[23] H. Bahl, W. Andersch, K. Braun, G. Gottschalk, Eur. J. Appl. Microbiol. Biotechnol. 14 (1982) 17–20.
[24] H. Bahl, W. Andersch, G. Gottschalk, Eur. J. Appl. Microbiol. Biotechnol. 15 (1982) 201–205.
[25] H. Janssen, C. Doring, A. Ehrenreich, B. Voigt, M. Hecker, H. Bahl, R.J. Fischer, Appl. Microbiol. Biotechnol. 87 (2010) 2209–2226.
[26] M.D. Jankowski, C.S. Henry, L.J. Broadbelt, V. Hatzimanikatis, Biophys. J. 95 (2008) 1487–1499.
[27] J.S. Youngleson, D.T. Jones, D.R. Woods, J. Bacteriol. 171 (1989) 6800–6807.
[28] S.A. Kim, L. Copeland, Appl. Environ. Microbiol. 63 (1997) 3432–3437.
[29] Y.L. Lin, H.P. Blaschek, Appl. Environ. Microbiol. 45 (1983) 966–973.
[30] J.-K. Guterl, V. Sieber, Eng. Life Sci. 13 (2013) 4–18.